

Optimal Placement of Superconducting Magnetic Energy Storages in a Distribution Network with Embedded Wind Power Generation

Steven Foday Sesay

Department of Electrical Engineering, Pan African University Institute for Basic Science, Technology and Innovation, Kenya
foday.steven@students.jkuat.ac.ke (corresponding author)

Cyrus Wabuge Wekesa

Department of Electrical Engineering, Pan African University Institute for Basic Science, Technology and Innovation, Kenya | School of Engineering, University of Eldoret, Kenya
cwekesa@uoeld.ac.ke

Livingstone M. H. Ngoo

Department of Electrical Engineering, Pan African University Institute for Basic Science, Technology and Innovation, Kenya | Department of Electrical Engineering, Multimedia University, Kenya
livingngoo@gmail.com

Received: 15 December 2023 | Revised: 15 January 2024 | Accepted: 28 January

Licensed under a CC-BY 4.0 license | Copyright (c) by the authors | DOI: <https://doi.org/10.48084/etasr.6754>

ABSTRACT

The prevalence of distributed generation in most power grids can negatively affect their performance in terms of power loss, voltage deviation, and voltage stability. Superconducting Magnetic Energy Storages (SMESs) can help in addressing this problem as long as they are optimally placed in the distribution network. This paper presents a hybrid Grasshopper Optimization Algorithm and a Simulated Annealing (GOA-SA) method to determine the optimal placement of SMESs in a distribution network with an embedded wind power generation system. The optimization was formulated as a multi-objective problem to minimize active power losses, reactive power losses, and voltage deviation and maximize the voltage stability index. An IEEE 57-node distribution network was employed and simulations were performed using MATLAB R2020b. Based on simulations using 200 kW SMESs in discharge mode, the active power loss decreased by 82.57%, the reactive power loss decreased by 80.71%, the average voltage deviation index decreased by 66.91%, and the voltage stability index improved by 34.97%. In the charging operation mode, the active power loss increased by 24.86%, the reactive power loss increased by 8.21%, the average voltage deviation increased by 12.86%, and the voltage stability index increased by 12.79%. These results show that SMESs can improve the technical performance of a distribution network.

Keywords-SMES; WTG; hybrid GOA-SA; optimal placement

I. INTRODUCTION

Stressed distribution networks lead to poor power quality, frequent power outages, high energy costs, and decreased reliability [1]. The amount of energy used today has grown significantly, whereas, at the same time, expenditures in the infrastructure supporting the power system and the use of fossil fuels have decreased. Conventional distribution networks have a strong hierarchical structure. However, the growing need for energy, the fast pace of technological development, fuel crises, blackouts, financial incentives, and public awareness of

environmental issues are pushing toward distributed energy resources with high reliability, stability, quality, and security. Today, Distributed Energy Resources (DERs) are a common component of many utilities worldwide and are increasingly integrated into power distribution networks. In addition to being environmentally friendly as green energy, their installation is crucial for the distribution network in terms of reduced power losses and improved voltage profile [2]. As renewable energy sources, such as wind power, are weather-dependent and erratic, they can affect the reliability of

distribution networks. An augmentation in load demand in a distribution network can result in a rise in voltage drop, which can impact power loss, voltage profile, and system stability. Distribution networks are rapidly integrating Energy Storage Systems (ESS) to address the aforementioned issues and offer other advantages. The former consists of flywheel storage [3], fuel cell storage [4], Compressed Air Energy Storage (CAES) [5], Compressed Carbon Dioxide Energy Storage (CCES) [6], Battery Energy Storage System (BESS) [7], and SMES [8]. Despite being the industry standard, BESSs have serious drawbacks, including a very short lifespan, voltage and current restrictions, potential environmental problems, and a slow response time. SMESs have several advantages over other ESS, involving long lifespan, no restrictions on the number of charging and discharging cycles, no moving components, high power density (0.1-10 MW), and high storage efficiency (95-98%) [9]. The primary disadvantage of an SMES is its high costs. The use of High-Temperature Superconductors (HTS) can lessen this drawback. HTSs are cooled with liquid nitrogen at 77°K, as opposed to 4.2°K for Low-Temperature Superconductors (LTS). Compared to LTSs, HTSs provide greater system reliability and fewer refrigeration expenses [10]. A recent review examined the design and development of high-temperature SMESs for power applications. Numerous studies have been performed on SMES cooling methods and thermal management techniques to reduce the degradation of superconductor performance at high temperatures, based on thermal energy storage materials. A Direct Current (DC) flowing through a superconducting coil can store electrical energy in the magnetic field it creates. The SMES coil can absorb or release real and reactive power based on the power demand of the distribution network. This power can be released in seconds to several hours, given that it is stored as a circulating current [11]. SMES can be utilized as energy storage in the distribution network to achieve several objectives, entailing improving power quality and transient voltage dips, controlling reactive power flow and voltage, stabilizing wind generators, spinning reserve, as well as minimizing power and voltage fluctuations of wind generators.

Several studies have investigated the effectiveness of SMES in ameliorating transient stability [12-16] and addressing variations in the output power and voltage of Wind Turbine Generators (WTGs) [17-19]. However, there is a lack of research on the optimal placement of SMESs in a power grid. In [20], a genetic algorithm was applied to optimally position an SMES in an IEEE 14-bus transmission system to enhance voltage stability, solely focusing on the voltage stability index. In [21], a method was presented to determine the optimal location of a superconducting device and so minimize system losses. This approach employed loss sensitivity analysis in a typical power system, considering a daily load profile, and exclusively focused on power loss when determining the optimal location of the SMES. In [22], a novel approach was presented to optimally place WTGs and SMESs in a distribution network, using the Equilibrium Optimizer (EO) and the loss sensitivity factor in the optimization process. This innovative method was applied to an IEEE 33-node distribution network. In [23], a technique was proposed for optimal placement of SMES and superconducting fault current

limiters in interconnected microgrids. The objective function included the voltage deviation of the doubly fed induction generator, the power deviation at the point of common coupling, the fault current in transmission lines, the features of the superconducting fault current limiter, and SMES, which were optimized utilizing the PSO algorithm.

This study proposes an optimal placement method for SMESs to minimize active and reactive power losses and voltage deviation and improve the voltage stability index. The hybrid Grasshopper Optimization Algorithm and Simulated Annealing (GOA-SA) technique were used in an IEEE 57-node distribution network with an embedded wind power generation system. The main contributions of this study are:

- Investigating the optimal placement of the SMES in the IEEE 57-node distribution network with an embedded wind power generation system considering four objective functions: active and reactive power losses, average voltage deviation, and voltage stability index.
- Improving the performance of the distribution network in terms of decreasing active and reactive power losses, voltage deviation, and voltage stability.
- Proposing a novel hybrid optimization algorithm and comparing it with its derivatives to solve optimization problems.
- Considering a distribution network with an embedded wind power generation system, representing a real-life scenario.

II. MATERIALS AND METHODS

A. Network Component Modeling

The model consists of the IEEE 57-node distribution network, SMES, and a wind power generation system.

1) IEEE 57-Node Distribution Network and Study Area

Figure 1 shows the single-line diagram of the IEEE 57-node distribution [24], with system voltages of 12.66 kV and total active and reactive power loads of 2694.600 kVA and 3802.190 kW, respectively. This system includes one slack bus, 57 buses, and 56 branches and load buses, correspondingly. The network is considered to be a residential/commercial network with 85% of the load being commercial loads.

2) SMES

From the power system point of view, an SMES can be seen as a generator, load, or storage system. SMES can be studied as a generator, constant charging equipment, a load, constant discharging equipment, and a storage device that can discharge and charge depending on the system's characteristics. This study examines the SMES as a generator and a load. Table I illustrates the generator (discharging) and load (charging) characteristics of the SMES, and its kW ratings are used to determine their optimal position [25-26].

3) Wind Power Generation System

The wind power generation system is modeled as a Type 3 Distributed Generator (DG) to incorporate its active and

reactive power consumption and injection capabilities [27]. The wind power generation system, known as WTG, has a penetration level of 30% [28]. Although there are several ways to calculate wind power penetration levels, the percentage of wind turbine penetration could be obtained as the ratio of [29]:

- The total production of the wind power generation systems to the total generation.
- The peak wind power generation capacity to the loads' peak apparent power.
- The wind-rated power to the loads' active power demand.

The penetration percentage of wind power was calculated utilizing the last method to determine the total wind-rated power needed for 30% penetration or 1125 kW. A Newton-Raphson load flow simulation was performed in MATLAB/PSAT to identify the chosen location of the WTG. Node 46 was selected as the location of the WTG in the distribution network.

TABLE I. DISCHARGING AND CHARGING CASES

Cases	Mode of Operation	Quantity
Case I	Discharge 100 kW power	3
Case II	Discharge 200 kW power	3
Case III	Charge 100 kW power	3
Case IV	Charge 200 kW power	3

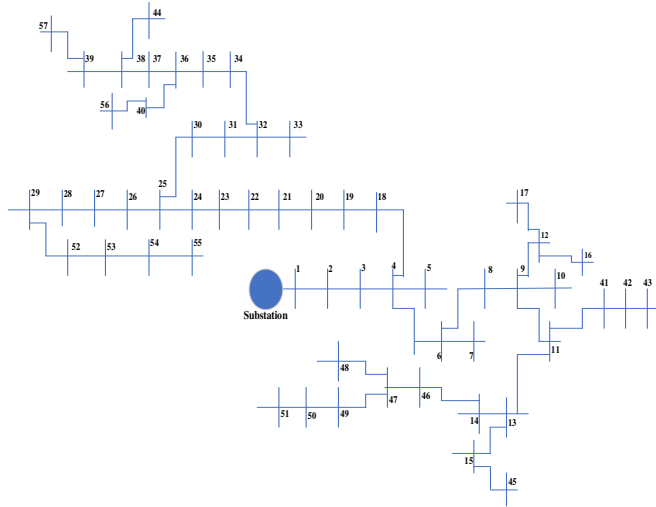


Fig. 1. Single line diagram for the IEEE 57-node distribution network.

B. Problem Formulation

The objective of this optimization problem is to minimize the active and reactive power losses of the network, the average voltage deviation index, and the voltage stability index when the SMESs are placed in the distribution network under discharging and charging conditions. Radial distribution networks have a large R/X ratio, and because of this, basic load flow tools such as Newton-Raphson or fast decoupled approaches do not provide accurate results. An efficient load flow method is presented based on the forward-backward method to solve the power flows of a radial distribution network [30-31].

1) Objective Function

a) Active and Reactive Power Loss Minimization

The active and reactive power losses in $P_{loss}(a, a+1)$ and $Q_{loss}(a, a+1)$ in a branch $a, a+1$ of the network is given by:

$$P_{loss(a,a+1)} = \left(\frac{P_{a+1}^2 + Q_{a+1}^2}{|V_{a+1}|^2} \right) * R_{br} \quad (1)$$

$$Q_{loss(a,a+1)} = \left(\frac{P_{a+1}^2 + Q_{a+1}^2}{|V_{a+1}|^2} \right) * X_{br} \quad (2)$$

where $P(a+1)$ and $Q(a+1)$ are the receiving end active and reactive powers, respectively, $V(i+1)$ is the receiving end voltage, R_{br} is the branch resistance, and X_{br} is the branch reactance. Therefore, the total power loss minimization function is given by:

$$f_1(j) = \min \sum_{b=1}^{br} [P_{loss}(b) + Q_{loss}(b)] \quad (3)$$

b) Minimization of Average Voltage Deviation Index (AVDI)

AVDI is the voltage deviation for 1.0 p.u., which is the reference voltage, and is defined in terms of the voltage magnitudes at all the nodes, given by:

$$f_2(j) = \frac{1}{N_i} \sum_{a=1}^{N_a} |1 - v_a|^2 \quad (4)$$

where N_a is the number of nodes in the network and v_a is the voltage at node a .

c) Maximization of the Voltage Stability Index (VSI)

At a receiving node b , VSI is given by:

$$f_3(j) = [|V_b|^4 - 4(P_b x_{ab} + Q_b r_{ab})^2 - 4(P_b r_{ab} + Q_b x_{ab})|V_b|^2] \quad (5)$$

where v_b is the voltage at node b , P_b is the active power demand at node b , Q_b is the reactive power demand at node b , r_{ab} is the resistance branch $a-b$, and x_{ab} is the reactance of branch $a-b$. Therefore, converting (1) into a minimization function and combining it with the former two equations gives the following multi-objective function:

$$F(j) = \min \left\{ w_1 f_1 + w_2 f_2 + w_3 \frac{1}{f_3(j)} \right\} \quad (6)$$

where w_1 , w_2 , and w_3 are weights assigned to the individual objective functions.

2) Constraints

The multi-objective function for this optimization problem is subject to the following constraints:

a) Power Balance (Equality Constraints)

The algebraic sum of all input and output active and reactive power flows through the system should be equal:

$$P_{sub} + \sum_{z=1}^{N_{WTG}} P_{WTG} + \sum_{z=1}^{N_s} P_{SMES} - \sum_{z=1}^{N_{br}} P_{Loss} - \sum_{z=1}^{N_{al}} P_L = 0 \quad (7)$$

$$Q_{sub} + \sum_{z=1}^{N_{WTG}} Q_{WTG} + \sum_{z=1}^{N_s} Q_{SMES} - \sum_{z=1}^{N_{br}} Q_{loss} - \sum_{z=1}^{N_{al}} Q_L = 0 \quad (8)$$

where P_{sub} and Q_{sub} represents substation active and reactive power, respectively, P_L and Q_L are active and reactive load demands, P_{loss} and Q_{loss} are active and reactive power losses in the z^{th} branch, P_{SMES} and Q_{SMES} are the active and reactive powers of the SMES, P_{WTG} and Q_{WTG} are the active and reactive powers of WTG [27].

b) Inequality Constraints

The voltage magnitude at each bus must be kept within an acceptable range at all times:

$$V_i^{min} \leq V_i \leq V_i^{max} \tag{9}$$

where V_{min} and V_{max} are the minimum and the maximum voltage limits. The current magnitude of each line I_r must remain within acceptable operating limits to avoid any excessive thermal stress of the line:

$$I_r \leq I_r^{max} \tag{10}$$

The maximum-minimum power limit constraint for SMES is:

$$P_s^{min} \leq P_s \leq P_s^{max} \tag{11}$$

and $P_s^{min} = P_s = P_s^{max}$ as the power rating of each SMES is fixed.

3) Grasshopper Optimization Algorithm (GOA)

GOA mimics the swarming behavior of grasshoppers. Each grasshopper in the swarm has its position that corresponds to a possible solution to the optimization problem [32]. X_i represents the position of the i^{th} grasshopper as:

$$X_i = S_i + G_i + A_i \tag{12}$$

where S_i is the social interaction, G_i is the force of gravity on the i^{th} grasshopper, and A_i is the wind advection. Social interaction is the dominant part all coming from grasshoppers themselves defined in:

$$S_i = \sum_{j=1}^N s(d_{ij}) \widehat{d}_{ij} \tag{13}$$

where N denotes the number of grasshoppers, $d_{ij} = |X_j - X_i|$ defines the Euclidean distance between the i^{th} and the j^{th} grasshopper, $\widehat{d}_{ij} = \frac{X_j - X_i}{d_{ij}}$ is a unit vector from the i^{th} to the j^{th} grasshopper, and s is a function to define the strength of social forces represented by:

$$s(r) = f \exp\left(\frac{-r}{l}\right) - \exp^{-r} \tag{14}$$

where f indicates the intensity of attraction, r is the force of repulsion, and l is the attractive length scale that has a value in $[0, 4]$ and controls the attraction or repulsion between grasshoppers. The area where there is no attraction or repulsion is called a comfort area. The comfort area exists at an exact distance of 2.079. The distance should be normalized to the interval $[1, 4]$, as the s function cannot handle strong forces with large distances. The G component has two parts, as g is the gravitational constant, and \widehat{e}_g shows a unity vector towards the center of the earth. The mathematical definition is given by:

$$G_i = -g \widehat{e}_g \tag{15}$$

The wind advection A_i is given by:

$$A_i = u \widehat{e}_w \tag{16}$$

where u represents the drift constant and \widehat{e}_w is a unit vector in the wind direction. Using components, (1) can be written as:

$$X_i = \sum_{j=1}^N s(|x_j - x_i|) \frac{x_j - x_i}{d_{ij}} - g \widehat{e}_g + u \widehat{e}_w \tag{17}$$

An improved version of this equation can be:

$$X_i^d = c \left(\sum_{j=1}^N c \frac{u_{bd} - l_{bd}}{2} s(|x_j^d - x_i^d|) \frac{x_j^d - x_i^d}{d_{ij}} \right) + \widehat{T}_d \tag{18}$$

where u_{bd} is the upper bound, l_{bd} is the lower bound in the d^{th} dimension and \widehat{T}_d is the value of the d^{th} dimension in the target (best solution found so far). The G component is ignored assuming no gravitational force and wind direction is always towards a target. The decreasing coefficient c is used twice in (18) for controlling forces between grasshoppers and is updated by (19). The outer c maintains the balance between exploration and exploitation, while the inner c reduces repulsion/attraction forces between grasshoppers proportional to the number of iterations.

$$c = c_{max} - l \frac{c_{max} - c_{min}}{L} \tag{19}$$

where $c_{max} = 1$ is the maximum value, $c_{min} = 0.00001$ is the minimum value, l indicates the current iteration, and L is the maximum number of iterations. GOA is extended by MOGOA to address multi-objective optimization problems. The target selection is based on crowding distance, similar to one in MOPSO [33] using:

$$P_i = \frac{1}{M_i} \tag{20}$$

where P_i is the probability of choosing the target from the archive and M_i is the number of solutions in the neighborhood of the i^{th} solution. Later this probability helps find the target using roulette wheel selection.

4) Simulated Annealing (SA)

SA is a stochastic search technique that originated from the principles of Monte Carlo simulation. This algorithm demonstrates the capability to effectively address complex combinatorial optimization problems. The annealing process involves simulating the thermal motion of atoms in the presence of a heat bath, where the temperature gradually decreases from a higher value to a lower one [34]. SA can avoid local optima by adjusting the temperature and modifying the solution according to a probability function:

$$P(\Delta E) = e^{\frac{-\Delta E}{TK_B}} \tag{21}$$

where K_B is Boltzmann's constant, T is the current temperature and ΔE is the change in the energies of atoms.

5) Hybrid Multiobjective GOA and SA

A new hybrid model of MOGOA was introduced, incorporating SA [33]. This approach involves mapping the position of the new grasshopper to the current optimal position within a symmetrical interval, which is determined by the product of the current temperature and a random number

mapped to the dimensional space. By applying SA, the algorithm can randomly alter the current value of the control parameter c . This adaptation helps improve the search process, leading to the discovery of high-quality solutions, as shown in:

$$C_{new} = C_{old} * (1 + ns) * e^{-ns \frac{1}{N}} \quad (22)$$

where C_{new} is the new perturb c , C_{old} is its value in the previous iteration, constant in the first iteration but later updated in every iteration, ns is the number of steps in SA, and N is the number of grasshoppers in the swarm. In the annealing process, the temperature is adjusted by:

$$T_{new} = T_{old} * \alpha \quad (23)$$

where α is the cooling coefficient which decreases temperature in each iteration. SA was used to change the value of inertia weight. When the fitness of the population increases, the new value of c is accepted, otherwise, the probability is calculated by applying the Gaussian probability function:

$$G(t) = \min \left(1.0, e^{-\left(\frac{fitness_{new} - fitness_{old}}{K_B T} \right)} \right) \quad (24)$$

where $fitness_{new}$ is the fitness after obtaining the new value of c using (12), $fitness_{old}$ is the fitness in the previous iteration, T is the annealing temperature, and K_B is Boltzmann's constant. The following equation changes c using $G(t)$ and the next iteration starts:

$$C_{new} = C_{old} * G(t) \quad (25)$$

The updated values of c obtained through the SA process are used in MOGOA to adjust the positions of grasshoppers. Through the optimization process, the SA search component aids the hybrid MOGOA in escaping local optima and reaching global solutions. Figure 2 displays a flowchart of the steps of the hybrid MOGOA and SA. These steps are summarized as follows:

- Step 1: Input the network line and bus data.
- Step 2: Run load flow calculation and record the results (power losses, node voltage, AVDI, VSI).
- Step 3: Place the WTG systems at the specified load, run load flow calculation, and record the results (power losses, node voltage, AVDI, VSI)
- Step 4: Initialize the MOGOA-SA parameters: Number of grasshoppers, maximum number of iteration, minimum value of c , maximum value of c , lower bound, upper bound, dimension, change in the energies of the atoms, number of steps in SA, cooling coefficient, and annealing temperature, as observed in Table II.
- Step 5: Calculate the fitness function of each search individual. The fitness function is evaluated by (6) for each individual.
- Step 6: Evaluate the population fitness using (21). The selection operator is then employed to choose parents for reproduction. With the crossover and mutation operators, new offspring are generated. The Pareto dominance

operator is utilized to identify non-dominated solutions, while the archive operator stores these Pareto-optimal solutions. The crowded distance operator is employed to maintain diversity within the population. The roulette wheel selection operator is engaged to select a target from the archive.

- Step 7: update coefficient c using (22) to achieve a balance between exploration and exploitation. Also, update the position of a current individual (i.e. the SMESs) using (25).
- Step 8: Output load flow results (power losses, node voltage, AVDI, VSI) and the optimal locations for the SMESs by checking the constraints and storing the solution according to the best fit. Then, update the best search individual and repeat steps 5, 6, and 7 until reaching the maximum iteration.

TABLE II. HYBRID MOGOA-SA PARAMETER VALUES

Parameters	Symbol	Values
Number of grasshoppers	N	10
Maximum number of Iteration	L	20
Minimum value of c	C_{min}	0.00004
Maximum value of c	C_{max}	0.1
Lower bound	l_{bd}	-7
Upper bound	u_{bd}	7
Dimension	d	2
Change in the energies of the atoms	ΔE	1.67
Number of steps in SA	ns	5
Cooling coefficient	α	0.95
Annealing temperature	T	200

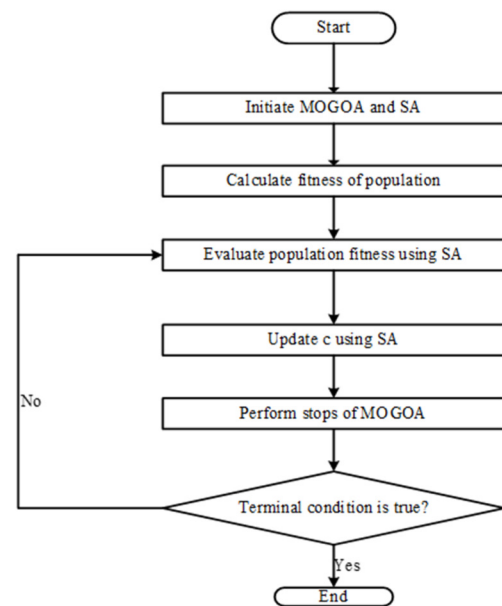


Fig. 2. Flowchart for hybrid MOGOA and SA.

III. RESULTS AND DISCUSSION

A. Optimal SMES Placement

Table III exhibits the optimal placement for the SMESs determined by the hybrid GOA-SA algorithm.

TABLE III. SUMMARY RESULTS FOR OPTIMAL PLACEMENT OF SMES

-	Base case	Case I	Case II	Case III	Case IV
Placement	-	47,22,8	14,10,25	47,22,8	14,10,25

TABLE IV. VOLTAGE MAGNITUDE FOR THE CASES

Node No.	Base Case	WTG	Case I	Case II	Case III	Case IV
1	0.999	0.999	0.999	1.020	0.961	0.929
2	0.999	0.999	0.999	1.017	0.961	0.928
3	0.999	0.999	0.999	1.013	0.961	0.928
4	0.999	0.999	0.999	1.002	0.961	0.928
5	0.999	0.999	0.999	1.001	0.961	0.928
6	0.999	0.997	0.999	1.000	0.961	0.928
7	0.998	0.989	0.989	1.000	0.960	0.928
8	0.998	0.976	0.989	1.000	0.960	0.928
9	0.998	0.975	0.989	1.000	0.960	0.913
10	0.999	0.973	0.990	1.000	0.961	0.913
11	0.995	0.972	0.986	1.000	0.957	0.913
12	0.993	0.970	0.984	1.000	0.955	0.913
13	0.984	0.964	0.975	1.000	0.946	0.910
14	0.986	0.962	0.977	1.000	0.948	0.901
15	0.987	0.961	0.978	1.000	0.949	0.901
16	0.986	0.960	0.977	1.000	0.948	0.901
17	0.985	0.957	0.976	1.000	0.947	0.900
18	0.984	0.957	0.975	1.000	0.946	0.900
19	0.983	0.957	0.974	1.000	0.945	0.900
20	0.982	0.956	0.973	1.000	0.944	0.900
21	0.981	0.956	0.972	1.000	0.943	0.900
22	0.985	0.956	0.976	1.000	0.947	0.900
23	0.982	0.956	0.973	1.000	0.944	0.909
24	0.980	0.956	0.971	0.998	0.942	0.909
25	0.981	0.956	0.972	0.997	0.943	0.909
26	0.979	0.955	0.970	0.989	0.941	0.920
27	0.978	0.955	0.969	1.000	0.940	0.920
28	0.976	0.955	0.967	1.000	0.938	0.923
29	1.000	1.000	0.991	1.000	0.962	0.923
30	0.999	0.999	0.999	1.000	0.961	0.923
31	0.999	0.999	0.999	1.000	0.961	0.923
32	0.999	0.999	0.999	1.000	0.961	0.923
33	0.999	0.999	0.999	1.000	0.961	0.923
34	0.999	0.999	0.999	1.000	0.961	0.923
35	0.999	0.999	0.999	1.000	0.961	0.923
36	0.999	0.999	0.999	1.000	0.961	0.923
37	0.999	0.999	0.999	1.000	0.961	0.923
38	0.998	0.999	0.989	1.000	0.960	0.923
39	0.998	0.999	0.989	1.000	0.960	0.923
40	0.998	0.999	0.989	1.000	0.960	0.923
41	0.996	0.998	0.987	1.000	0.958	0.923
42	0.995	0.996	0.986	1.000	0.957	0.923
43	0.995	0.997	0.986	1.000	0.957	0.923
44	0.993	0.997	0.984	1.000	0.955	0.923
45	0.988	0.996	0.979	1.000	0.950	0.923
46	0.987	0.996	0.978	1.000	0.949	0.923
47	0.994	0.994	0.985	1.000	0.956	0.923
48	0.994	0.994	0.985	1.000	0.956	0.923
49	0.993	0.993	0.984	1.000	0.955	0.921
50	0.993	0.993	0.984	1.000	0.955	0.921
51	0.992	0.987	0.983	1.000	0.954	0.921
52	0.991	0.975	0.982	1.000	0.953	0.920
53	0.990	0.971	0.981	1.000	0.952	0.918
54	0.987	0.967	0.978	1.000	0.949	0.916
55	0.984	0.962	0.975	1.000	0.946	0.914
56	0.985	0.940	0.976	1.000	0.947	0.909
57	0.984	0.930	0.975	1.000	0.946	0.901

It was assumed that the optimal placement obtained for the discharge operations of SMESs is the same as for the charging operation. Cases I and II have moderately dispersed SMESs. The reason behind this could be that, in the discharging operation, an effective minimization of active power loss, reactive power loss, AVDI, and maximum VSI might occur. This can cause a minimal deterioration in technical performance, which is expected in the charging mode of operation of the SMESs.

1) Network Voltage Profile

The network voltage magnitude for all four simulation cases is shown in Table IV. Introducing the WTG at a 30% penetration level into the distribution network leads to deterioration of the voltage profile, with a minimum voltage of 0.930 p.u. at node 57. When the SMESs are placed in the network in the discharge mode of operations, improvement is noticed in cases I and II. This improvement in the network voltage magnitude is a result of the SMESs serving as generators, thereby counteracting the drop in the voltage magnitudes. Maximum voltage magnitude of 1.020 p.u. at node 1 and minimum voltage magnitude of 0.989 p.u. at node 26 are obtained. In the charging mode of operation for case II, it was assumed that the SMESs are in the optimal location, as in the discharge case. Cases III and IV have a minimum voltage magnitude of 0.901 p.u. at node 57. It was observed that the voltage magnitude of the nodes in the network drops as the sizes of the SMESs increase from 100kW to 200kW. Using the hybrid GOA-SA algorithm, we can say that when SMESs are placed optimally, there is significant improvement in the voltage magnitude during the discharging modes of operation of the SMESs.

2) Average Voltage Deviation Index (AVDI)

The VDI of a node can be defined as the difference between the actual voltage value seen at the node and the reference voltage, which is often represented as 1 p.u. The average VDI value across all network nodes is used to compute AVDI. A decrease in value corresponds to an increase in the voltage stability of the network. Table V shows that the base case's AVDI increased by 30.08% as an outcome of WTG being integrated into the network, since it rose from 0.0186 in the base case to 0.0266 when the WTG was embedded at node 46. When SMESs are optimally placed using the proposed GOA-SA method and operate in the discharge mode, the AVDI for Case I was 0.0132, reduced by 50.86%. In Case II, the AVDI was 0.0088, reduced by 66.91%. In the charging mode, the AVDI for Case III was 0.0278, and for Case IV was 0.0289, increasing by 9.02 and 12.86%, respectively.

TABLE V. AVERAGE VOLTAGE DEVIATION INDEX

Scenario	Case I	Case II	Case III	Case IV
Base Case	0.0186	0.0186	0.0186	0.0186
WTG	0.0266	0.0266	0.0266	0.0266
WTG+SMES	0.0132	0.011	0.0278	0.0289

3) Voltage Stability Index (VSI)

VSI measures network stability. The network's voltage and current magnitudes drive the VSI to estimate the distance between the operating point of the current and the collapse

point of the voltage [35]. As it decreases, the network's vulnerability to voltage instability increases. A greater VSI value raises network stability, unlike VDI. Table VI portrays the minimum VSIs obtained from the simulation.

TABLE VI. MINIMUM VOLTAGE STABILITY INDEX

Scenario	Case I	Case II	Case III	Case IV
Base Case	0.739	0.739	0.739	0.739
WTG	0.735	0.735	0.735	0.735
WTG+SMES	0.931	0.988	0.728	0.671

VSI decreased by 14.14%, from 0.839 to 0.735, as a result of the WTG's integration into the network. During the discharge mode of the SMESs, for Case I, the minimum VSI was 0.931, increased by 26.67%. In Case II, the minimum VSI was 0.988, increased by 34.97%. In the charging mode, for Case III, the minimum VSI was 0.702, reduced by 4.49%. In Case IV, the minimum VSI was 0.641, reduced by 12.79%. The reduction in the minimum VSI of the network occurs as the size of SMESs increases under the charging mode of operation. The placement of SMESs using the GOA-SA method improved the net VSI of the network.

4) Active and Reactive Power Losses

In each simulation case, the integration of the WTG results led in a significant reduction in the overall active power loss, as it decreased from 158.06 to 56.11 kW, reducing the active power loss by 64.43% for the four cases, as illustrated in Table VII. In the discharging mode of operation of SMESs, for Case I, the active power loss decreased by 76.03%, from 56.11 to 13.45 kW. In Case II, the active power loss decreased by 82.57%, from 56.11 to 9.78 kW. In the charging mode of operation for Case III, the active power loss increased by 14.86%, from 56.11 to 64.45 kW. In Case IV, the active power loss increased by 24.86%, from 56.11 to 70.06 kW.

Table VIII indicates that in the discharging mode of SMESs, the reactive power loss increased by 24.88%, from 99.86 to 75.01 kVar, when the WTG was incorporated into the network. This is because WTG can generate reactive power as well as active power. When SMESs are optimally placed in the

network for Case I, the reactive power loss decreased by 67.26%, from 75.01 to 24.56 kVar. In Case II, the reactive power loss decreased by 80.71%, to 14.56 kVar. In the charging mode of operation of SMESs, for Case III, the reactive power loss increased by 6.18%, from 75.01 to 58.78 kVar. In Case IV, reactive power loss increased by 8.21%, to 81.16 kVar. The active and reactive power losses under both discharging and charging modes of operation were less compared to the base case.

TABLE VII. TOTAL ACTIVE POWER LOSS

Cases	Base Case (kW)	WTG (kW)	WTG+SMES (kW)
Case I	158.654	56.11	13.45
Case II	158.654	56.11	9.78
Case III	158.654	56.11	64.45
Case IV	158.654	56.11	70.06

TABLE VIII. TOTAL REACTIVE POWER LOSS

Cases	Base Case (kVar)	WTG (kVar)	WTG +SMES (kVar)
Case I	99.86	75.01	24.56
Case II	99.86	75.01	14.56
Case III	99.86	75.01	58.78
Case IV	99.86	75.01	81.16

B. Validation of the Proposed Hybrid GOA-SA

Tables IX and X show the comparison of the proposed hybrid GOA-SA algorithm for the optimal placement of SMESs in a distribution network with embedded wind power generation systems with GOA and SA independently for the same objective. The proposed method for placing SMESs leads to reduced active power losses, reactive power losses, AVDI, and an improved VSI. In contrast to using the algorithms independently, their hybrid usage results in lower active and reactive power losses, reduced voltage deviation, and improved VSI. These findings demonstrate the effectiveness of the proposed hybrid GOA-SA in identifying the optimal nodes for SMESs. Furthermore, this shows the efficiency of the proposed hybrid method in leveraging the strengths of one algorithm to address the limitations of the other.

TABLE IX. COMPARISON OF THE RESULTS OBTAINED FOR DISCHARGE OPERATIONS USING CASES I AND II

Algorithms	Case I						Case II					
	Opt. Location	Min Volt (p.u)	kW Loss	kVar Loss	Min VSI	AVDI	Opt. Location	Min Volt (p.u)	kW Loss	kVar Loss	Min VSI	AVDI
GOA- SA	47,22,8	0.9890	13.45	23.56	0.931	0.0132	14,10,25	0.9970	9.78	14.54	0.988	0.0088
GOA	47,23,9	0.9768	13.71	25.03	0.927	0.0143	7,20,31	0.9871	10.34	15.12	0.979	0.0098
SA	23,45,12	0.9618	14.32	24.56	0.928	0.0139	19,8,34	0.9862	11.73	14.83	0.968	0.0120

TABLE X. COMPARISON OF THE RESULTS OBTAINED FOR DISCHARGE OPERATIONS USING (CASES III AND IV)

Algorithms	Case III						Case IV					
	Opt. Location	Min Volt (p.u)	kW Loss	kVar Loss	Min VSI	AVDI	Opt. Location	Min Volt (p.u)	kW Loss	kVar Loss	Min VSI	AVDI
GOA-SA	47,22,8	0.9294	64.45	79.34	0.702	0.0279	14,10,25	0.9000	70.05	81.16	0.0641	0.0289
GOA	47,23,9	0.9133	66.23	80.58	0.701	0.0286	7,20,31	0.8951	72.19	83.26	0.0638	0.0293
SA	23,45,12	0.9324	67.59	82.09	0.689	0.0286	19,8,34	0.898	73.00	83.29	0.0636	0.0297

IV. CONCLUSION AND RECOMMENDATIONS

This study focused on the optimal placement of SMESs in a distribution network with embedded WTGs using a novel

hybrid GOA-SA optimization technique, considering four objective functions: active and reactive power losses, AVDI, and VSI. The objective was to optimally place SMESs to significantly improve the technical performance when

discharging, while considering its effect under the charging mode of operations using 100 and 200 kW SMESs. Integrating WTGs into the network significantly reduces the active and reactive power losses, but deteriorates the voltage profile in the network. The 200 kW SMESs in the discharge mode of operations performed the best in reducing active power losses, reactive power losses, and average voltage deviations and improved VSI. However, this resulted in a higher deterioration in the aforementioned technical parameters under the charging mode of operations. The novel hybrid GOA-SA method clearly shows its effectiveness in optimally placing SMESs in the network compared to GOA and SA independently. This concept can be utilized to determine the optimal placement of the SMESs for maximum savings in system operation costs.

ACKNOWLEDGEMENT

Steven Foday Sesay wishes to acknowledge the African Union Commission for his scholarship.

REFERENCES

- [1] M. J. Burke and J. C. Stephens, "Political power and renewable energy futures: A critical review," *Energy Research & Social Science*, vol. 35, pp. 78–93, Jan. 2018, <https://doi.org/10.1016/j.erss.2017.10.018>.
- [2] S. M. Said, A. Selim, and B. Hartmann, "Enhancement of voltage profile for unbalanced distribution system with wind energy and superconducting magnetic energy storage," in *2018 International Conference on Innovative Trends in Computer Engineering (ITCE)*, Aswan, Egypt, Feb. 2018, pp. 289–295, <https://doi.org/10.1109/ITCE.2018.8316640>.
- [3] A. H. Yakout, H. M. Hasanien, and H. Kotb, "Proton Exchange Membrane Fuel Cell Steady State Modeling Using Marine Predator Algorithm Optimizer," *Ain Shams Engineering Journal*, vol. 12, no. 4, pp. 3765–3774, Dec. 2021, <https://doi.org/10.1016/j.asej.2021.04.014>.
- [4] W. Buckles and W. V. Hassenzahl, "Superconducting magnetic energy storage," *IEEE Power Engineering Review*, vol. 20, no. 5, pp. 16–20, May 2000, <https://doi.org/10.1109/39.841345>.
- [5] X. Luo, J. Wang, M. Dooner, J. Clarke, and C. Krupke, "Overview of Current Development in Compressed Air Energy Storage Technology," *Energy Procedia*, vol. 62, pp. 603–611, Jan. 2014, <https://doi.org/10.1016/j.egypro.2014.12.423>.
- [6] F. Chaychizadeh, H. Dehghandorost, A. Aliabadi, and A. Taklifi, "Stochastic dynamic simulation of a novel hybrid thermal-compressed carbon dioxide energy storage system (T-CCES) integrated with a wind farm," *Energy Conversion and Management*, vol. 166, pp. 500–511, Jun. 2018, <https://doi.org/10.1016/j.enconman.2018.04.050>.
- [7] R. Sadiq, Z. Wang, C. y. Chung, C. Zhou, and C. Wang, "A review of STATCOM control for stability enhancement of power systems with wind/PV penetration: Existing research and future scope," *International Transactions on Electrical Energy Systems*, vol. 31, no. 11, 2021, Art. no. e13079, <https://doi.org/10.1002/2050-7038.13079>.
- [8] M. H. Qais, H. M. Hasanien, and S. Alghuwainem, "Output power smoothing of wind power plants using self-tuned controlled SMES units," *Electric Power Systems Research*, vol. 178, Jan. 2020, Art. no. 106056, <https://doi.org/10.1016/j.epr.2019.106056>.
- [9] M. H. Ali, B. Wu, and R. A. Dougal, "An Overview of SMES Applications in Power and Energy Systems," *IEEE Transactions on Sustainable Energy*, vol. 1, no. 1, pp. 38–47, Mar. 2010, <https://doi.org/10.1109/TSTE.2010.2044901>.
- [10] E. A. Gouda, A. Abd-Alaziz, and M. El-Saadawi, "Design modeling, and control of multi-stage SMES integrated with PV system," *Journal of Energy Storage*, vol. 29, Jun. 2020, Art. no. 101399, <https://doi.org/10.1016/j.est.2020.101399>.
- [11] M. C. Argyrou, P. Christodoulides, and S. A. Kalogirou, "Energy storage for electricity generation and related processes: Technologies appraisal and grid scale applications," *Renewable and Sustainable Energy Reviews*, vol. 94, pp. 804–821, Oct. 2018, <https://doi.org/10.1016/j.rser.2018.06.044>.
- [12] H. M. Hasanien and S. M. Muyeen, "Particle Swarm Optimization-based Superconducting Magnetic Energy Storage for Low-voltage Ride-through Capability Enhancement in Wind Energy Conversion System," *Electric Power Components and Systems*, vol. 43, no. 11, pp. 1278–1288, Jul. 2015, <https://doi.org/10.1080/15325008.2015.1027017>.
- [13] H. M. Hasanien, S. Q. Ali, and S. M. Muyeen, "Wind generator stability enhancement by using an adaptive artificial neural network-controlled superconducting magnetic energy storage," in *2012 15th International Conference on Electrical Machines and Systems (ICEMS)*, Sapporo, Japan, Oct. 2012.
- [14] S. M. Said and B. Hartmann, "Alleviation of Extremely Power and Voltage Variations Caused by Wind Power and Load Demand Using SMES," *Periodica Polytechnica Electrical Engineering and Computer Science*, vol. 63, no. 3, pp. 134–143, Mar. 2019, <https://doi.org/10.3311/PPee.13718>.
- [15] M. H. Ali, T. Murata, and J. Tamura, "Transient Stability Enhancement by Fuzzy Logic-Controlled SMES Considering Coordination With Optimal Reclosing of Circuit Breakers," *IEEE Transactions on Power Systems*, vol. 23, no. 2, pp. 631–640, May 2008, <https://doi.org/10.1109/TPWRS.2008.920045>.
- [16] R. Khanna, G. Singh, and T. K. Nagsarkar, "Artificial neural network based SMES unit for transient stability improvement," in *2010 Joint International Conference on Power Electronics, Drives and Energy Systems & 2010 Power India*, New Delhi, India, Sep. 2010, pp. 1–7, <https://doi.org/10.1109/PEDES.2010.5712476>.
- [17] W. Kreeumporn and I. Ngamroo, "Optimal Superconducting Coil Integrated Into PV Generators for Smoothing Power and Regulating Voltage in Distribution System With PHEVs," *IEEE Transactions on Applied Superconductivity*, vol. 26, no. 7, Jul. 2016, <https://doi.org/10.1109/TASC.2016.2591981>.
- [18] T. Chaiyatham and I. Ngamroo, "Optimal Fuzzy Gain Scheduling of PID Controller of Superconduction Magnetic Energy Storage for Power System Stabilization," *International Journal of Innovative Computing, Information and Control*, vol. 9, no. 2, pp. 651–666, Feb. 2013.
- [19] A. Boudia, S. Messalti, A. Harrag, and M. Boukhniher, "New hybrid photovoltaic system connected to superconducting magnetic energy storage controlled by PID-fuzzy controller," *Energy Conversion and Management*, vol. 244, Sep. 2021, Art. no. 114435, <https://doi.org/10.1016/j.enconman.2021.114435>.
- [20] X. Huang, G. Zhang, and L. Xiao, "Optimal Location of SMES for Improving Power System Voltage Stability," *IEEE Transactions on Applied Superconductivity*, vol. 20, no. 3, pp. 1316–1319, Apr. 2010, <https://doi.org/10.1109/TASC.2010.2044988>.
- [21] S. J. Lee, "Location of a Superconducting Device in a Power Grid for System Loss Minimization Using Loss Sensitivity," *IEEE Transactions on Applied Superconductivity*, vol. 17, no. 2, pp. 2351–2354, Jun. 2007, <https://doi.org/10.1109/TASC.2007.898435>.
- [22] M. Hashem, M. Abdel-Salam, M. Th. El-Mohandes, M. Nayel, and M. Ebeed, "Optimal Placement and Sizing of Wind Turbine Generators and Superconducting Magnetic Energy Storages in a Distribution System," *Journal of Energy Storage*, vol. 38, Jun. 2021, Art. no. 102497, <https://doi.org/10.1016/j.est.2021.102497>.
- [23] A. Komijani, M. Kheradmandi, and M. Sedighzadeh, "Optimal Allocation and Control of Superconducting Fault Current Limiter and Superconducting Magnetic Energy Storage in Mesh Microgrid Networks to Improve Fault Ride Through," *Journal of Operation and Automation in Power Engineering*, vol. 11, no. 1, pp. 22–32, Apr. 2023, <https://doi.org/10.22098/foape.2023.9577.1668>.
- [24] M. M. Ansari, C. Guo, M. S. Shaikh, N. Chopra, I. Haq, and L. Shen, "Planning for Distribution System with Grey Wolf Optimization Method," *Journal of Electrical Engineering & Technology*, vol. 15, no. 4, pp. 1485–1499, Jul. 2020, <https://doi.org/10.1007/s42835-020-00419-4>.
- [25] I. Hadjipaschalis, A. Poullikkas, and V. Efthimiou, "Overview of current and future energy storage technologies for electric power applications," *Renewable and Sustainable Energy Reviews*, vol. 13, no. 6, pp. 1513–1522, Aug. 2009, <https://doi.org/10.1016/j.rser.2008.09.028>.

- [26] Y. Huang, Y. Ru, Y. Shen, and Z. Zeng, "Characteristics and Applications of Superconducting Magnetic Energy Storage," *Journal of Physics: Conference Series*, vol. 2108, no. 1, Aug. 2021, Art. no. 012038, <https://doi.org/10.1088/1742-6596/2108/1/012038>.
- [27] A. D. Petropoulos, N. C. Koutsoukis, E. S. Karapidakis, and P. S. Georgilakis, "Optimal Mix of Wind Generation and Energy Storage Systems in Power Distribution Networks," presented at the MedPower 2014, Athens, Greece, Nov. 2014, <https://doi.org/10.1049/cp.2014.1640>.
- [28] Y. Kassem, H. Gokcekus, H. Camur, and A. H. A. Abdelnaby, "Wind Power Generation Scenarios in Lebanon," *Engineering, Technology & Applied Science Research*, vol. 12, no. 6, pp. 9551–9559, Dec. 2022, <https://doi.org/10.48084/etasr.5258>.
- [29] S. Sulaeman, F. T. Alharbi, M. Benidris, and J. Mitra, "A new method to evaluate the optimal penetration level of wind power," in *2017 North American Power Symposium (NAPS)*, Morgantown, WV, USA, Sep. 2017, pp. 1–6, <https://doi.org/10.1109/NAPS.2017.8107332>.
- [30] V. K. B. Ponnampalani and K. Swarnasri, "Multi-Objective Optimal Allocation of Electric Vehicle Charging Stations and Distributed Generators in Radial Distribution Systems using Metaheuristic Optimization Algorithms," *Engineering, Technology & Applied Science Research*, vol. 10, no. 3, pp. 5837–5844, Jun. 2020, <https://doi.org/10.48084/etasr.3517>.
- [31] T. N. Ton, T. T. Nguyen, A. V. Truong, and T. P. Vu, "Optimal Location and Size of Distributed Generators in an Electric Distribution System based on a Novel Metaheuristic Algorithm," *Engineering, Technology & Applied Science Research*, vol. 10, no. 1, pp. 5325–5329, Feb. 2020, <https://doi.org/10.48084/etasr.3372>.
- [32] L. Abualigah and A. Diabat, "A comprehensive survey of the Grasshopper optimization algorithm: results, variants, and applications," *Neural Computing and Applications*, vol. 32, no. 19, pp. 15533–15556, Oct. 2020, <https://doi.org/10.1007/s00521-020-04789-8>.
- [33] F. Sajjad *et al.*, "An efficient hybrid approach for optimization using simulated annealing and grasshopper algorithm for IoT applications," *Discover Internet of Things*, vol. 3, no. 1, Jul. 2023, Art. no. 7, <https://doi.org/10.1007/s43926-023-00036-3>.
- [34] M. O. Genc and N. Kaya, "Vibration Damping Optimization using Simulated Annealing Algorithm for Vehicle Powertrain System," *Engineering, Technology & Applied Science Research*, vol. 10, no. 1, pp. 5164–5167, Feb. 2020, <https://doi.org/10.48084/etasr.3242>.
- [35] M. S. S. Danish, T. Senju, S. M. S. Danish, N. R. Sabory, N. K., and P. Mandal, "A Recap of Voltage Stability Indices in the Past Three Decades," *Energies*, vol. 12, no. 8, Jan. 2019, Art. no. 1544, <https://doi.org/10.3390/en12081544>.